Multi-pass absorption spectroscopy for H_2O_2 detection using a CW DFB-QCL

[1]Yingchun Cao, [2]Nancy P. Sanchez, [1]Wenzhe Jiang, [3]Wei Ren, [1]Rafał Lewicki, [1]Dongfang Jiang, [2]Robert J. Griffin, and [1*]Frank K. Tittel

[1]Rice University, Electrical and Computer Engineering Department, 6100 Main St. Houston, TX, 77005, USA

[2] Rice University, Civil and Environmental Engineering Department, 6100 Main St. Houston, TX, 77005, USA

[3] Chinese University of Hong Kong, Mechanical and Automation Engineering Department, New Territories, Hong Kong

[*]fkt@rice.edu

Abstract: Hydrogen peroxide (H_2O_2) detection was demonstrated with multi-pass absorption spectroscopy using a commercial 76-m astigmatic multi-pass absorption cell. A ~7.73 μm continuous wave, distributed feedback quantum cascade laser (CW DFB-QCL) was employed for targeting a strong H_2O_2 line (1296.2 cm^{-1}) in the fundamental absorption band. Wavelength modulation spectroscopy combined with a second harmonic detection technique was utilized to increase the signal-to-noise ratio. By optimizing the pressure inside the multi-pass cell and the wavelength modulation depth, a minimum detection limit of 13.4 ppbv was achieved for H_2O_2 with a 2-s sampling time. From an Allan-Werle deviation plot, the detection limit could be improved to 1.5 ppbv with an averaging time of 200 s. Interference effects of atmospheric air components are also discussed.

OCIS codes: (280.3420) Laser sensors; (300.6340) Spectroscopy, infrared; (140.5965) Semiconductor lasers, quantum cascade; (120.4640) Optical instruments.

1. Introduction

Hydrogen peroxide (H_2O_2) is an important atmospheric trace gas that is formed mainly by combination of hydroperoxyl radicals [1]. H_2O_2 acts as a reservoir for HO_x radicals (e.g., OH and HO_2) and therefore plays an important role in the oxidative capacity of the atmosphere. Furthermore, H_2O_2 participates in the formation of sulfate aerosol by in-cloud oxidation of S(IV) to S(VI), which is closely linked with the phenomena of acid fog and rain [2-4]. Due to its high reactivity and low concentration (ppbv to sub-ppbv levels [5-7]), the detection of atmospheric H_2O_2 involves specific challenges.

Traditional approaches for determination of H_2O_2 in the atmosphere are often based on wet-chemistry techniques, in which transfer of H_2O_2 from the

gas phase to the liquid phase is required for subsequent determination by techniques such as fluorescence spectroscopy [8, 9]. Sampling artifacts and interferences from other atmospheric constituents may be introduced in these methods and can cause an additional error in the H_2O_2 concentration determination. Therefore direct concentration measurements of gas-phase H_2O_2 offers significant practical advantages.

Tunable diode laser absorption spectroscopy (TDLAS) is a widely used tool for gas detection due to its high sensitivity and selectivity. Gas-phase H_2O_2 detection based on TDLAS has been reported by several research groups. Slemr et al. demonstrated gas phase H_2O_2 measurement by using a 40-m multi-pass White cell, and reported a detection limit of 2.9 ppbv with a 5-minute averaging time [10]. Lindley et al. utilized a quantum cascade laser (QCL)-based TDLAS technology using a 100.1-m astigmatic multi-pass cell (MPC) and obtained a H_2O_2 detection limit of 15 and 3 ppbv for walkthrough portal and optical bench top instruments, respectively [11]. However, the large number of co-added spectra complicates data processing and increases the data acquisition time. Another TDLAS system with a H_2O_2 detection limit of 110 pptv for a 1 s averaging time was demonstrated by McManus et al. [12]. Their low detection limit was obtained using a long path-length gas absorption cell (260 m with 554 passes). More recently H_2O_2 detection based on a sensitive quartz-enhanced photoacoustic spectroscopy technique with a continuous wave (CW), distributed feedback (DFB) QCL was reported by our group. With this H_2O_2 sensor, detection limits of 75 ppbv for a 1 s sampling time and of 12 ppbv for 100 s averaging time were achieved [13]. Other spectroscopic methods such as cavity-enhanced optical frequency comb spectroscopy have been demonstrated for gas-phase H_2O_2 detection with a detection limit of 130 ppb in the presence of 2.8% water [14].

In this paper, a TDLAS-based sensor system capable of sensitive, selective gas-phase H_2O_2 detection and using a CW DFB QCL targeting a strong H_2O_2 absorption line at ~1296.2 cm^{-1} was demonstrated.

2. Experimental configuration

The H_2O_2 sensor system is depicted in Figure 1. A thermoelectrically cooled (TEC) CW DFB-QCL (Corning Inc., New York) operating at 7.73 μm was used as the excitation laser source. The laser wavelength was tuned with a temperature controller (TED 200C, Thorlabs, Inc.) to coincide with the targeted H_2O_2 absorption line. In addition, a low frequency sawtooth wave and a high frequency sinusoidal wave provided by a function generator (AFG 3102, Tektronix, Inc.) were combined and sent to a current controller (LDX 3232, ILX Lightwave) to realize QCL wavelength scanning and modulation across the H_2O_2 absorption line, respectively.

The CW-DFB-QCL beam was directed to a wedged beam splitter and focused by three plano-convex lenses, L_1 (f=50 mm), L_2 (f=100 mm) and L_3

(f=250 mm), at the center of a commercial multi-pass gas absorption cell (AMAC-76, Aerodyne Research, Inc.). A pinhole (D=400 μm) was employed between L_1 and L_2 to further improve the beam shape and meet the optical requirement of the MPC. The QCL beam exiting from the MPC was collected by a parabolic mirror and directed to a mid-infrared detector (PVMI-3TE-8, Vigo System S.A.). The electric signal from this detector was demodulated by a lock-in amplifier and acquired with a data acquisition (DAQ) card (DAQCard-AI-16XE-50, National Instruments). The two reflected beams from the beam splitter were utilized for wavelength locking and power normalization, respectively. One of the reflected beams is passed through a reference gas cell containing 1% N_2O at a pressure of 150 Torr and was detected by a pyroelectric detector (LIE-332f, InfraTec) to reduce the noise associated with QCL wavelength drifts. The QCL wavelength was locked to a N_2O absorption line at 1296.27 cm^{-1} in order to target the adjacent optimum H_2O_2 absorption line (1296.2 cm^{-1}). The reflected beam also was detected by a second IR detector (PVM-10.6, Vigo System S.A.) to monitor the presence of potential QCL power variations. The H_2O_2 gas flow entering the MPC was controlled using a pressure controller (MKS, Inc #649) and an oil free vacuum pump (KNF, #N813.5).

3. System optimization and selection of the target H_2O_2 absorption line

3.1 Laser beam optimization

A critical step in the design of a MPC-based gas sensor system is to optimize the coupling of the QCL beam into the gas cell with minimum optical noise introduced due to scattered light at the entrance and exit MPC holes and beam interference inside the MPC. The MPC used in our system is an Aerodyne, Inc. AMAC-76 astigmatic Herriott cell with a volume of 0.5 liters and mechanical length of 32 cm [15]. The laser beam was focused at the center of the MPC, with a working distance larger than half of the cell length. In our H2O2 sensor system, three plano-convex lenses were used to reshape the laser beam and focus the beam efficiently into the MPC as mentioned in Section 2. The QCL beam size was calculated by means of the Gaussian beam equation [16] along the propagation direction and shown (red curve) in Figure. 2. The separation distances are 148 mm between L_1 and L_2 and 100 mm between L_2 and L_3. The focusing point at the center of the MPC is 270 mm from L_3, with a beam waist <1 mm. The experimental beam evolution was recorded using an IR camera (PV320, Electrophysics Corp.) at several positions and shown in Figure 2. The beam sizes at these positions agree well with the theoretical design. To eliminate the imperfect pattern of the initial laser beam (inset in Figure 2 prior to L_1), a pinhole with a diameter of 400 μm is inserted at the focal point of lens L_1 as a spatial filter. A QCL beam with circular shape was obtained at the focal point of lens L_3.

3.2 MPC optical path-length verification

A visible red laser beam co-aligned with the QCL beam was injected after the wedged beam splitter to facilitate the alignment of the mid-infrared QCL beam through the MPC. After adjusting the entrance angle of the incoming red laser beam, the correct beam pattern, resulting in 238 passes between the MPC mirrors, was obtained for the MPC and shown as an inset in Figure 3. An effective path-length of 76 m was obtained with this alignment. To verify this MPC path-length, a cylinder containing 5.4 ppm methane (CH_4) was used to measure the absorption in the MPC at ~1297.5 cm^{-1} and at a pressure of 100 Torr. The effective absorption length agreed with the expected optical path-length within ±1% by comparing the CH_4 transmission peaks with the HITRAN database [17].

3.3 H_2O_2 line selection and optimization

H_2O_2 absorption lines in the ν_6 fundamental ro-vibrational band in the 7.4-8.4 μm spectral range were considered to be optimum due to their strong absorption. Figure 4(a) depicts a HITRAN-based absorption spectrum [17] simulated for 1 ppm gas-phase H_2O_2 (red line) balanced by pure N_2 at 296 K and 30 Torr within a 1295.95-1296.3 cm^{-1} spectral range. The absorption spectrum of air is also presented in Figure 4 for comparison. It is found that there are two groups of strong H_2O_2 absorption lines, labeled as single-peak (1296.01 cm^{-1}) and double-peak (1296.2 cm^{-1}) in this spectral region that show a small overlap with interference from absorption peaks in air. These two groups of peaks were selected as suitable H_2O_2 lines for further measurements. Experimental second harmonic (2*f*) signals of H_2O_2, air and pure N_2 were recorded using wavelength modulation spectroscopy with the second harmonic (2*f*-WMS) detection method, as shown in Figure 4(b). The strong single-peak and double-peak of H_2O_2 could be easily distinguished from the curve with very low interferences from air constituents.

In order to achieve a better system detection sensitivity, the pressure inside the MPC and the modulation depth for WMS should be optimized [18,19]. Gas-phase H_2O_2 with a fixed concentration was generated by mixing an air flow with H_2O_2 vapor generated by a closed container filled with a 10% H_2O_2 solution. For each individual pressure ranging from 30 Torr to 250 Torr, the 2*f* signals for both single-peak (open circles) and double-peak (solid dots) were recorded with a 5-kHz modulation frequency and different modulation depths as shown in Figure 5(a). According to Figure 5(a) the maximum signal for the single-peak is achieved for a 5-mA modulation depth at 150 Torr, while that for the double-peak is obtained for a modulation depth of 8 mA at 150 Torr. To better understand this behavior, the entire 2*f* signal curves are plotted in Figure 5(b) for several pressure and modulation depth combinations. It was found that at low pressures (<100 Torr), the H_2O_2 peaks are broadened with increasing pressure and modulation depth, and the peak amplitude value for

the single-peak is slightly higher than that of the double-peak for each individual operation combination. However, when the pressure is increased, the double-peak becomes a single wide peak due to the line-broadening effect, which results in a large increase for the peak amplitude value. From these data, the optimal operation conditions for the H_2O_2 sensor system were determined to be an 8-mA modulation depth and a 150-Torr pressure.

4. System performance and discussion

A 2*f*-WMS method was utilized to carry out the H_2O_2 concentration measurements. The wavelength of the QCL was tuned to the double-peak of H_2O_2 at ~1296.2 cm^{-1} (240 mA, 27 °C). Two current signals, with sawtooth (10 mA, 0.5 Hz) and sinusoidal (8 mA, 5 kHz) waves, were combined and sent to the current controller to realize both laser wavelength scanning and modulation at the same time. The DC part of the main detector output was recorded to show the transmission of the MPC, while the AC part was delivered to the lock-in amplifier for 2*f* signal demodulation. The pressure inside the MPC was controlled at 150 Torr for maximum signal generation.

4.1 Sensitivity calibration

The sensitivity calibration of the sensing system was carried out by mixing the air flow with the H_2O_2 vapor produced by a 30% H_2O_2 solution (w/w). As it takes several minutes for the H_2O_2 concentration to reach a constant level in the MPC, several groups of data for both the transmissions and the 2*f* signals were recorded at constant time intervals during the period of concentration stabilization. The H_2O_2 concentrations are calibrated by fitting the transmission curves to the standard HITRAN transmission values with the same operating conditions [17]. A lock-in amplifier time constant of 50 ms was selected for optimal 2*f* signal demodulation within the 2-s ramp period. The 2*f* signal curves across the target H_2O_2 line for H_2O_2 concentrations from 0.5 ppm to 10 ppm are plotted in Figure 6(a). The peak values for different H_2O_2 concentration signals are plotted in Figure 6(b). The fit shows linear relationship with a R^2 value greater than 0.999 and a proportionality coefficient of k = 0.9297 mV/ppm. The intercept of 0.2469 mV originates from the baseline.

4.2 Noise level analysis

The noise level analysis of our system was accomplished based on Allan – Werle variance [20]. To avoid the noise induced by absorption change, we used pure N_2 as the detection gas. The 2*f* magnitude in terms of H_2O_2 concentration at the double-peak position was monitored for ~3 hours, as shown in Figure 7(a). An Allan-Werle deviation analysis is employed for investigating the long-term stability and precision of the H_2O_2 measurements for the reported H_2O_2 detection system, as shown in Figure 7(b). A minimum detection limit (MDL) (1σ) of 13.4 ppbv was achieved for H_2O_2 with our

sensor system at a 2-s sampling time. If the averaging time is increased to an optimal value of 200 s, the MDL can be improved to 1.5 ppbv, as deduced from the Allan deviation plot.

These results were verified by evaluating the sensor system at low H_2O_2 concentration levels. A ppbv-level H_2O_2 concentration was generated by passing an air flow over 0.1% H_2O_2 solution (w/w) with a constant flow rate of 300 cm^3/min. The H_2O_2 vapor concentration in the mixed gases was estimated to be ~30 ppb according to the sensitivity calibration described in Sec. 4.1. After a period of time, the H_2O_2 solution was consecutively exchanged with pure water. The 2*f* signals in terms of H_2O_2 concentration for these changes are plotted in Figure 8, where 30 ppb H_2O_2 corresponds to the environment of 0.1% H_2O_2 solution mixed with air flow and zero air shows the pure water vapor mixed with air flow (background). This figure clearly shows the change in the measured H_2O_2 concentration levels when switching between the 30 ppb H_2O_2 and zero gas mixtures. With increased averaging time, as indicated by red and green lines in Figure 8, these changes become more evident, indicating that a lower detection limit can be obtained with a longer averaging time, as expected from Figure. 7. The response time for a H_2O_2 concentration change for consecutive environment alternation is ~120 s. This long time response is due to the absorption/adsorption of H_2O_2 onto the MPC walls and gas lines. Appropriate treatments such as coating the glass surface of the MPC with a layer of special material in order to limit the adsorption effects [21], or heating the gas cell with a temperature controllable thermal tape, can lead to a significant reduction in this response time.

4.3 Atmospheric H_2O_2 detection limit determined by gas interference

As discussed in Sec. 3.3, the double-peak of H_2O_2 at ~1296.2 cm^{-1} was selected as the target absorption feature due to its line strength and limited overlapping with other molecules present in the atmospheric air. In laboratory measurements, the concentrations of air components are relatively constant, and the prepared H_2O_2 concentration can generally ensure a large SNR. In this case, there is no significant concern about a potential gas interference issue. However, for in-field atmospheric H_2O_2 measurements, the low concentration of H_2O_2 (~ppb to sub-ppb in the atmosphere) and unpredictable variations in concentration of air components may introduce significant challenges for H_2O_2 environmental measurements. Therefore, the gas interference might be an important factor that the limits final system behavior and potential application in field campaigns.

For our system, where the pressure is controlled to 150 Torr, the line broadening effect will enhance this interference. In order to show the interferences from other atmospheric gases that have absorption features within the laser tuning range, the absorption spectra of H_2O, N_2O, and CH_4 were simulated at 150 Torr using the HITRAN database and are plotted in

Figure 9(a). For comparison, the absorption lines for air and 1 ppm H_2O_2 also are depicted. It is shown that the interferences from air components are considerable for both the double-peaks and single-peaks. These absorption lines also are simulated at a lower pressure of 38 Torr as shown in Figure 9(b). As expected, the interferences of air components become less significant due to decrease in line width. Table 1 presents the interferences of air components on selected H_2O_2 line positions at different pressures. These values represent the equivalent H_2O_2 concentrations with absorptions equal to that of a 10% concentration change for each air component. Table 1 shows that for a 150 Torr pressure, H_2O is the major interfering species, and the change in absorption for the double-peak resulting from a 10% H_2O concentration change in air is equal to a concentration variation of ~43 ppb H_2O_2. For the single-peak, this value (~26.6 ppb) is also much greater than the atmospheric H_2O_2 concentration. However, as the pressure decreases to 38 Torr, these interference effects are reduced significantly, resulting in a total interference of 3.2 ppb for a single-peak and 8 ppb for a double-peak. However, in this case the MDL of the system will become much larger due to the significant signal loss, as indicated in Figure 5, which will prevent the sensor from being able to quantify atmospheric H_2O_2 concentrations.

Based on the above discussion, the selected H_2O_2 absorption line at 1296.2 cm^{-1} for our sensor system might not be able to realize accurate atmospheric H_2O_2 detection due to the limited sensitivity and interference from air components. By investigating all the H_2O_2 absorption lines in the mid-infrared spectral region, an optimum H_2O_2 line at 1249.45 cm^{-1} appears as a better candidate for H_2O_2 detection due to its strong absorption and ultra-small interference from air constituents. The absorption curves of this optimum H_2O_2 line are presented in Fig. 9(c) at pressures of 150 Torr and 38 Torr with a path-length of 76 m. The interference from atmospheric air is negligible at the optimum H_2O_2 line position. The equivalent H_2O_2 concentration changes caused by a 10% air component concentration change are presented in Table 1 for comparison. The interferences from air result in ppt-level H_2O_2 concentration changes, which are much smaller than the atmospheric H_2O_2 concentration. Therefore, our sensor system targeting this optimum H_2O_2 line (1249.45 cm^{-1}) with an appropriate QCL wavelength could achieve atmospheric H_2O_2 detection overcoming potential interferences from air.

5. Conclusions

A H_2O_2 detection system based on multi-pass absorption spectroscopy was demonstrated. A 7.73-μm CW DFB-QCL was used to target the strong H_2O_2 absorption line at 1296.2 cm^{-1} in the ν_6 fundamental absorption band. An astigmatic Herriott MPC with an effective optical path-length of 76 m was employed to measure low H_2O_2 concentrations. Wavelength modulation spectroscopy with second harmonic detection was utilized to achieve optimum

H_2O_2 detection sensitivity. A MDL of 13.4 ppbv for H_2O_2 concentration measurement was achieved with an acquisition time of 2 s. This value could be improved to 1.5 ppbv after implementing an integration time of 200 s based on an Allan-Werle deviation analysis. Furthermore, observed interference effects due to atmospheric air components are discussed for different conditions to provide insight into potential limitations of using mid-infrared multi-pass absorption spectroscopy for atmospheric H_2O_2 detection. Finally, an optimum H_2O_2 absorption line at 1249.45 cm^{-1} (~8 μm) was suggested for even better performance of the sensor system.

Acknowledgments

The authors gratefully acknowledge the financial support from a National Science Foundation (NSF) ERC MIRTHE award, a NSF-ANR award for international collaboration in chemistry, "Next generation of Compact Infrared Laser based Sensor for Environmental Monitoring (NexCILAS)" and the Robert Welch Foundation grant C-0586.

References

1. W. R. Stockwell, "On the HO_2 + HO_2 reaction: its misapplication in atmospheric chemistry models," J. Geophys. Res. **100**(D6), 11695-11698 (1995).
2. B. J. Finlayson-Pitts and J. N. Pitts Jr., *Chemistry of the Upper and Lower Atmosphere - Theory, Experiments, and Applications.* (Academic, San Diego, 2000).
3. S. A. Penkett, B. J. Bandy, C. E. Reeves, D. McKenna, and P. Hignett, "Measurements of peroxides in the atmosphere and their relevance to the understanding of global tropospheric chemistry," Faraday Discuss. **100**, 155-174 (1995).
4. D. Vione, V. Maurino, C. Minero, and E. Pelizzetti, "The atmospheric chemistry of hydrogen peroxide: A review," Ann. Chim. **93**(4), 477-488 (2003).
5. R. Balasubramanian and L. Husain, "Observations of gas-phase hydrogen peroxide at an elevated rural site in New York," J. Geophys. Res. - Atmos. **102**(D17), 21209-21220 (1997).
6. V. P. Aneja and M. Das, "Correlation of ozone and meteorology with hydrogen peroxide in urban and rural regions of North Carolina," J. Appl. Meteorol. **34**, 1890-1898 (1995).
7. T. Yamashita, H. Sakugawa, and K. Fujiwara, "Measurements of hydrogen peroxide in the atmosphere and rainwater in Hiroshima and Higashi-Hiroshima, Japan," Nippon Kagaku Kaishi **12**, 1127-1133 (1994).
8. H. Sakugawa, I. R. Kaplan, W. Tsai, and Y. Cohen, "Atmospheric Hydrogen Peroxide," Environ. Sci. Technol. **24**(10), 1452-1462 (1990).
9. M. Lee, B. G. Heikes, and D. W. O'Sullivan, "Hydrogen peroxide and organic hydroperoxide in the troposphere: A review," Atmos. Environ. **34**, 3475-3494 (2000).
10. F. Slemr, G. W. Harris, D. R. Hastie, G. I. Mackay, and H. I. Schiff , "Measurement of gas phase hydrogen peroxide in air by tunable diode laser absorption spectroscopy," J. Geophys. Res. Atmos. **91**(D5), 5371-5378 (1986).
11. R. Lindley, E. Normand, M. McCulloch, P. Black, I. Howieson, C. Lewis, and B. Foulger, "Bulk and trace detection of ammonia and hydrogen peroxide using quantum cascade laser technology - a tool for identifying improvised explosive devices," Proc. SPIE **7119**, 71190K (2008).

12. J. B. McManus, M. S. Zahniser, and D. D. Nelson, "Dual quantum cascade laser trace gas instrument with astigmatic Herriott cell at high pass number," Appl. Opt. **50**(4), A74-A85 (2011).
13. W. Ren, W. Jiang, N.P. Sanchez, P. Patimisco, V. Spagnolo, C. Zah, F. Xie, L. C. Hughes, R. J. Griffin, F. K. Tittel, "Hydrogen peroxide detection with quartz-enhanced photoacoustic spectroscopy using a distributed-feedback quantum cascade laser," Appl. Phys. Lett. **104**, 041117 (2014).
14. A. Foltynowicz, P. Masłowski, A. J. Fleisher, B. J. Bjork, and J. Ye, "Cavity-enhanced optical frequency comb spectroscopy in the mid-infrared application to trace detection of hydrogen peroxide," Appl. Phys. B **110**, 163-175 (2013).
15. J. B. McManus, P. L. Kebabian, and M. S. Zahniser, "Astigmatic mirror multipass absorption cells for long-path-length spectroscopy," Appl. Opt. **34**(18), 3336-3348 (1995).
16. H. Kogelnik and T. Li, "Laser Beams and Resonators," Appl. Opt. **5**(10), 1550-1567 (1966).
17. L. S. Rothman, I. E. Gordon, A. Barbe, D. Chris Benner, P. F. Bernath, M. Birk, V. Boudon, L. R. Brown, A. Campargue, J.-P. Champion, K. Chance, L. H. Coudert, V. Dana, V. M. Devi, S. Fally, J.-M. Flaud, R. R. Gamache, A. Goldman, D. Jacquemart, I. Kleiner, N. Lacome, W. J. Lafferty, J.-Y. Mandin, S. T. Massie, S. N. Mikhailenko, C. E. Miller, N. Moazzen-Ahmadi, O. V. Naumenko, A. V. Nikitin, J. Orphal, V. I. Perevalov, A. Perrin, A. Predoi-Cross, C. P. Rinsland, M. Rotger, M. Šimečková, M. A. H. Smith, K. Sung, S. A. Tashkun, J. Tennyson, R. A. Toth, A. C. Vandaele, and J. Vander Auwera, "The HITRAN 2008 molecular spectroscopic database," J. Quant. Spectrosc. Radiat. Transf. **110**(9-10), 533-572 (2009).
18. P. Werle, "A review of recent advances in semiconductor laser based gas monitors," Spectrochim. Acta A **54**(2), 197-236 (1998).
19. S. Schilt, L. Thévenaz, and P. Robert, "Wavelength modulation spectroscopy: combined frequency and intensity laser modulation," Appl. Opt. **42**(33), 6728-6738 (2003).
20. P. Werle, R. Mücke, and F. Slemr, "The limits of signal averaging in atmospheric trace-gas monitoring by tunable diode-laser absorption spectroscopy (TDLAS)," Appl. Phys. B **57**(2), 131-139 (1993).
21. J. B. McManus, J. H. Shorter, D. D. Nelson, and M. S. Zahniser, "Compact quantum cascade laser instrument for rapid, high sensitivity measurements of trace gases in air," Sensors, 2007 IEEE, 1341-1344 (2007).

Figures and Table

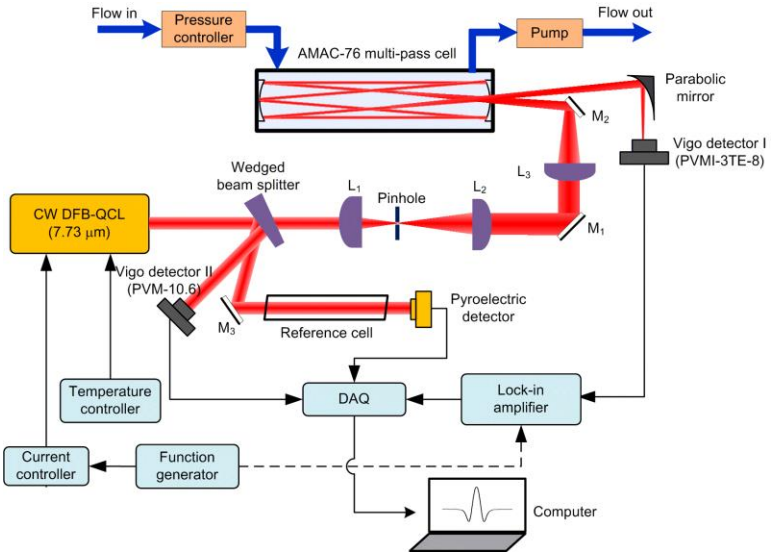

Figure 1. Schematic of the H_2O_2 sensor system. L: lens, M: mirror, DAQ: data acquisition.

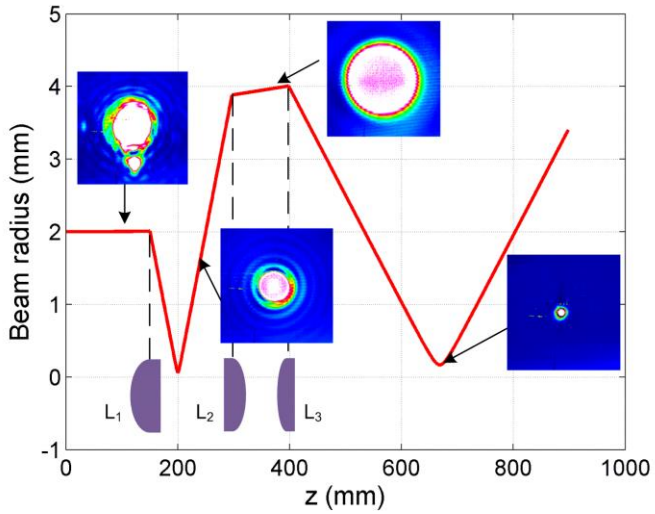

Figure 2. Laser beam radius evolution resulting from the use of three plano-convex lenses, L_1 (f=50 mm), L_2 (f=100 mm) and L_3 (f=250 mm). The red curve is the theoretical beam radius variation along the propagation direction, the inset beam patterns were measured by an IR camera, and the dashed line indicates the positions of the three lenses .

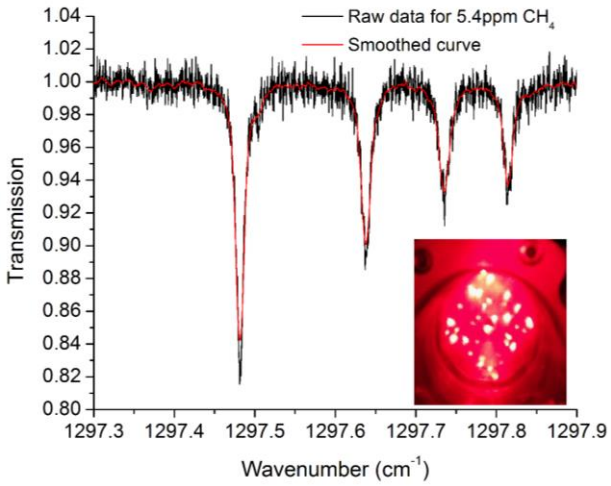

Figure 3. Experimentally measured transmission curve of 5.4 ppm CH_4 with the MPC used in our system at 100 Torr. The inset figure shows the trace laser beam pattern observed on the front mirror of the MPC.

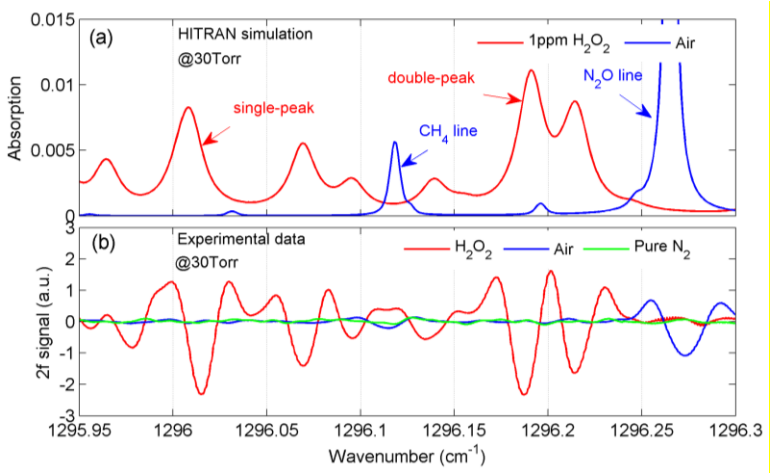

Figure 4. H_2O_2 absorption spectra and air at a pressure of 30 Torr. (a) CH_4 and N_2O absorption results from the HITRAN database; (b) 2*f* signals from experimental measurements. Single-peak and double-peaks represent two groups of strong H_2O_2 absorption lines at ~1296.01 cm^{-1} and ~1296.2 cm^{-1}, respectively.

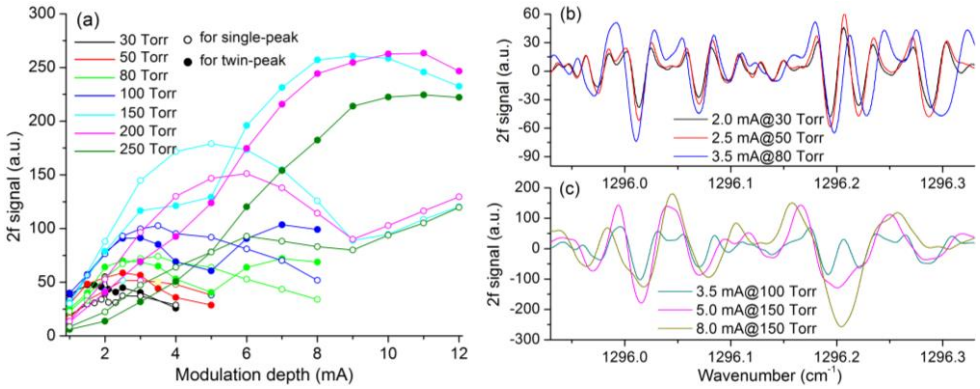

Figure 5. (a) Peak values of 2*f* signals at single-peak (open circles) and double-peak (solid dots) for different pressures and modulation depths; (b) 2*f* signal curves for different operating conditions at lower pressures; (c) 2*f* signal curves for different operating conditions at higher pressures.

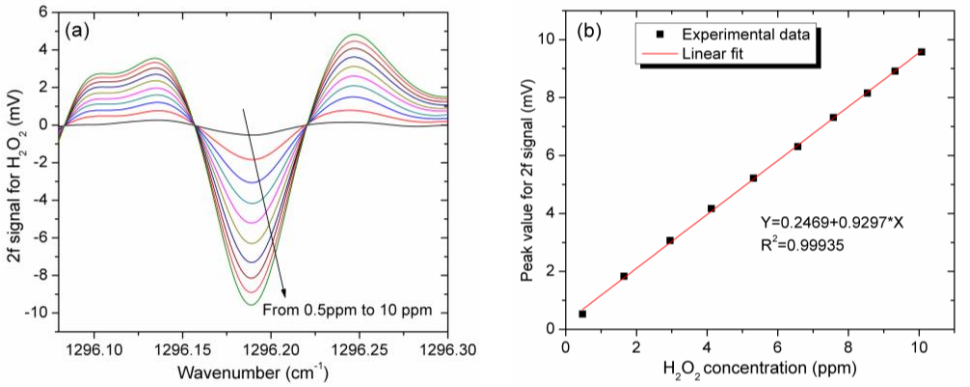

Figure 6. Calibration for the H_2O_2 detection system. (a) 2*f* signals for different H_2O_2 concentrations as the laser wavelength is scanned across the double-peak; (b) Peak 2*f* signals versus H_2O_2 concentration values.

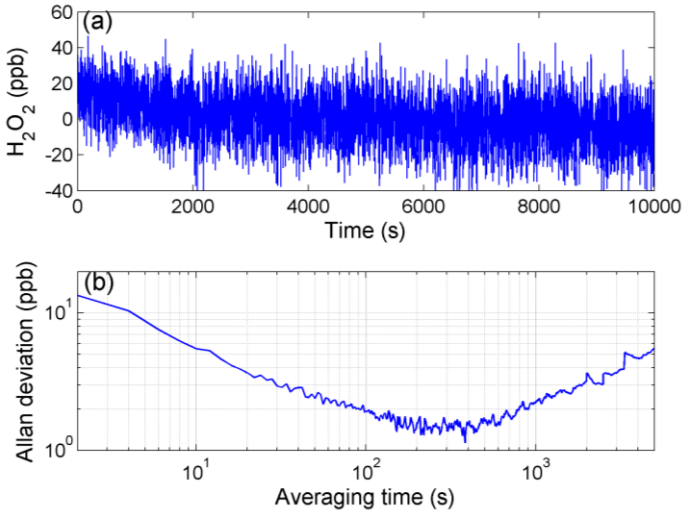

Figure 7. (a) Signal in terms of the H_2O_2 concentration with pure N_2; (b) Allan deviation in ppb for the signal in Figure 7(a) as a function of the averaging time.

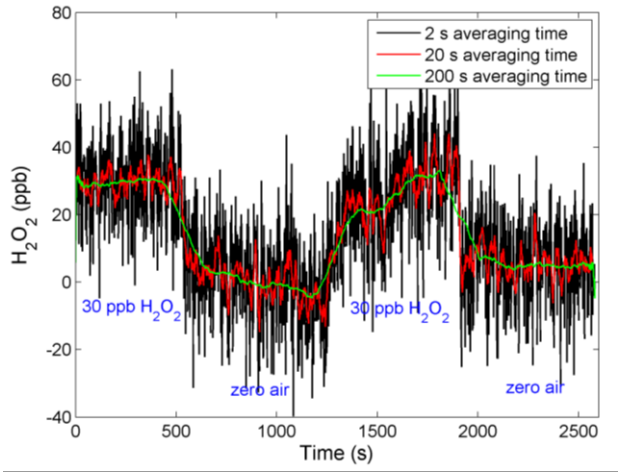

Figure 8. Low H_2O_2 concentration measurements. Lines with different colors show the measured signal behavior of our system at different averaging times.

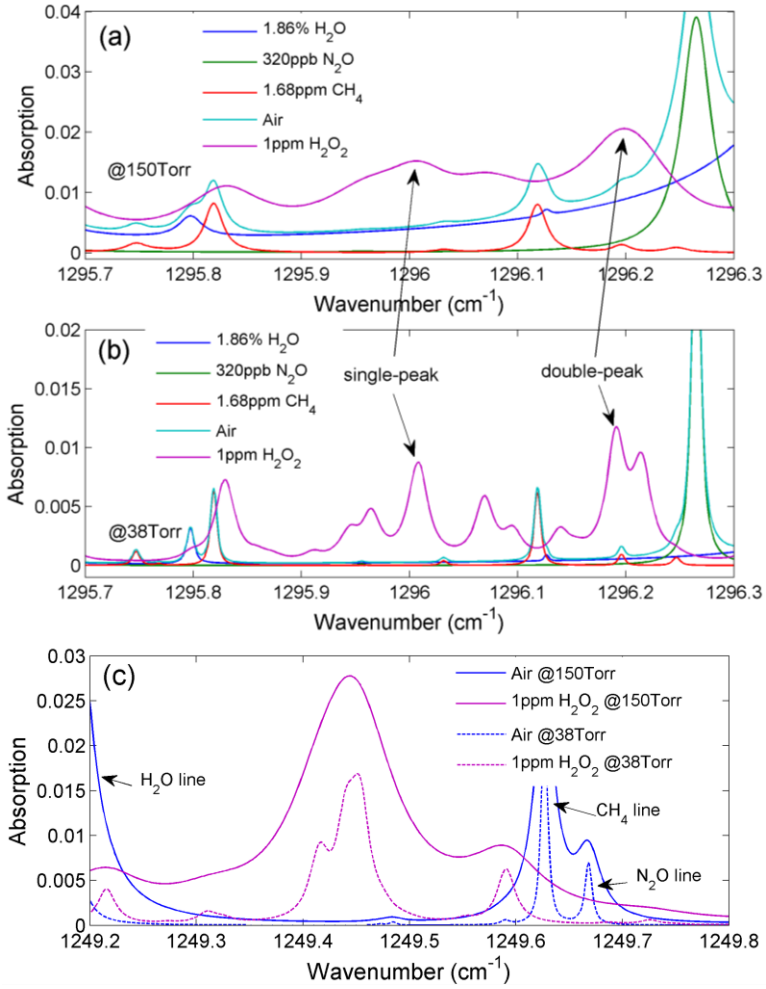

Figure 9. Interference effects of individual air components (H_2O, N_2O, CH_4 and air) adjacent to H_2O_2 absorption lines acquired with a 76-m path-length at pressures of (a) 150 Torr and (b) 38 Torr; (c) optimum H_2O_2 absorption line at ~1249.45 cm^{-1} compared with air absorption at 150 and 38 Torr for an absorption length of 76 m.

Table 1. Equivalent H_2O_2 concentrations in ppb due to a 10% concentration change of air components at a single-peak absorption (1296.01 cm^{-1}), double-peak absorption (1296.2 cm^{-1}), and the optimum H_2O_2 absorption (1249.45 cm^{-1}) positions.

H_2O_2 lines	P (Torr)	1.86% H_2O	320 ppb N_2O	1.68 ppm CH_4
Single-peak line (1296.01 cm^{-1})	38	2.90	0.15	0.15
	75	9.57	0.52	0.51
	112	17.83	0.99	0.92
	150	26.58	1.49	1.29
Double-peak line (1296.2 cm^{-1})	38	4.53	0.99	2.50
	75	14.40	3.40	7.51
	112	27.40	6.82	6.69
	150	43.01	10.48	6.60
Optimum H_2O_2 absorption line (1249.45 cm^{-1})	38	0.031	0.015	0.030
	75	0.131	0.058	0.121
	112	0.295	0.125	0.270
	150	0.523	0.221	0.500